Volume 8, Number 6 (December 2015) p. 787-799 • ISSN 1983-4195
http://dx.doi.org/10.1590/S1983-41952015000600004

REVISTA IBRACON DE ESTRUTURAS E MATERIAIS
IBRACON STRUCTURES AND MATERIALS JOURNAL

Experimental and finite element analysis of bond-slip in reinforced concrete

Análises experimental e por elementos finitos da perda de aderência em concreto armado

A. R. V. WOLENSKI [a]
andersonwolenski@gmail.com

S. S. DE CASTRO [a]
saullo9@yahoo.com.br

S. S. PENNA [a]
spenna@dees.ufmg.br

R. L. S. PITANGUEIRA [a]
roquepitangueira@gmail.com

B. V. SILVA [b]
dovalesilva@hotmail.com

M. P. BARBOSA [c]
mbarbosa@dec.feis.unesp.br

Abstract

The modeling of reinforced concrete structures has taken advantage of the increasing progress on Computational Mechanics, in such way that complex phenomena, such as cracking and crushing, creep, reinforcement yielding, steel-concrete bond loss, can be modeled in a reasonable realistic way, using the proper set of numerical and computational resources. Among several options, the ones based on the Finite Element Method (FEM) allow complex analysis simulations of reinforced concrete structures, including the interaction of different nonlinear effects. This paper deals with the nonlinear finite element analysis of the bond-slip between reinforcing steel and concrete, taking into account an experimental study previously performed. The FEM analysis presented uses a combination of resources where the material behavior of concrete is described by the Microplane Constitutive Model, and an embedded reinforcement model is used to represent steel inside the concrete and take into account the effect of bond-slip. The FEM models were created using the INSANE (INteractive Structural ANalysis Environment) computational system, open source software that has a set of FEM tools for nonlinear analysis of reinforced concrete structures. The correlations between numerical-experimentals results and several parameters validate the proposed combination of resources and identifies the significance of various effects on the response.

Keywords: reinforced concrete structures, microplane constitutive models, embedded reinforcement, bond-slip.

Resumo

A modelagem de estruturas de concreto armado tem tido um crescente progresso na Mecânica Computacional, de modo que os fenômenos complexos, tais como fissuração e esmagamento, fluência, escoamento da armadura, perda da aderência aço-concreto, podem ser modelados de forma razoavelmente realista, usando um conjunto apropriado de recursos numéricos e computacionais. Entre as diversas opções, os baseados no Método dos Elementos Finitos (MEF) permitem simulações complexas de análises de estruturas de concreto armado, incluindo a interação de diferentes efeitos não lineares. Este artigo lida com a análise não linear em elementos finitos, da perda de aderência entre a armadura de aço e o concreto, levando em consideração um estudo experimental anteriormente realizado. A análise via MEF apresentada usa uma combinação de recursos onde o comportamento do concreto é descrito pelo Modelo Constitutivo de Microplanos, e um Modelo de Armadura Embutida é usado para representar o aço inserido no concreto e levar em conta o efeito da perda de aderência. Os modelos do MEF foram criados usando o sistema computacional INSANE (Interactive Structural Analysis Environment), software de código aberto que possui um conjunto de ferramentas para análise não linear de estruturas em concreto armado. As correlações entre os resultados numérico-experimentais e os vários parâmetros validam a combinação de recursos proposta e identificam o significado de vários efeitos sobre a resposta.

Palavras-chave: estruturas de concreto armado, modelos constitutivos de microplanos, armadura embutida, perda de aderência.

[a] *Universidade Federal de Minas Gerais (UFMG), Programa de Pós-Graduação em Engenharia de Estruturas (PROPEEs), Belo Horizonte, MG, Brasil;*
[b] *Universidade do Extremo Sul Catarinense, Departamento de Engenharia Civil, PPGCEM, Criciúma, SC, Brasil;*
[c] *Univesidade Estadual Paulista, Departamento de Engenharia Civil, Ilha Solteira, Brasil.*

Received: 24 Jun 2015 • Accepted: 11 Sep 2015 • Available Online: 24 Nov 2015

1. Introduction

Reinforced concrete is the most important building material and it is widely used in modern structures. So, theoretical and experimental researches become more and more necessary in order to develop advanced analysis methods.

Experimental research provides the basis for the theoretical models and also supplies the basic information for the analysis methods, such as material properties. In addition, the results of analysis methods have to be evaluated by comparing them with experiments.

Theoretical research can reduce the number of required test specimens for the solution of a given problem. The development of analytical models for reinforced concrete structures is complicated because of its complex behavior that includes: cracking and crushing, creep, reinforcement yielding, steel-concrete bond failure, among others phenomena.

However, nowadays, the modeling of reinforced concrete structures has taken advantage of the increasing progress on Computational Mechanics, in such way these complex phenomena can be modeled, in a reasonable realistic way, using o proper set of numerical and computational resources.

One of the most powerful methods of structural analysis is the Finite Element Method (FEM), which allows complex numerical simulations of reinforced concrete structures, including the interaction of different nonlinear effects.

This paper deals with the Finite Element Analysis of the bond-slip between reinforcing steel and concrete, taking into account the experimental study previously performed by Silva [1].

The FEM models were created using the *INSANE* (*Interactive Structural Analysis Environment*) computational system, open source software available at *www.insane.dees.ufmg.br*. The current version of *INSANE* has a set of FEM tools for nonlinear analysis of reinforced concrete structures, such as: (1) extensive library of analysis models and incremental-iterative methods for solving nonlinear equations; (2) an unified computational environment for constitutive models; and (3) FEM models for reinforcement and bond-slip.

Among these tools, the FEM analysis presented in this paper uses an appropriate combination of resources. The material behavior of concrete is described by the Microplane Constitutive Model, briefly described in section 2. An embedded reinforcement model is used to represent steel inside a concrete element and take into account the effect of bond-slip (section 3). The experimental program is detailed in section 4. In section 5, both pullout tests and finite element simulations are presented and the results from the two are compared.

2. Microplane model

The application of Microplane Theory (Mohr [2], Taylor [3]) to modeling concrete structures is quite pertinent because the association between solid structure of the heterogeneous material (cementitious matrix with aggregates of different particle sizes) and the existence of multiple plans of discontinuities positioned at the interfaces of its grains (Figure 1).

Although this association has been understood on a micro scale, Bažant and Gambarova [4] formulated a macro scale model based on such association. The model prescribes constitutive behavior in individual and independent microplanes and relates this local behavior with macro stresses and strains in order to represent the inelastic response of the material. After this pioneer work, many other microplane models has been proposed (Carol [5], Ožbolt [6], Carol [7], Leukart [8], Leukart and Ramm [9]). All of them follow the schema showed in Figure 2.

In a very general way, the formulation of Microplane Models follows three main steps, as can be seen in Fig. 2. Given the macroscopic strain tensor at a material point, kinematic constraints are imposed in order to calculate the strains on the microplanes. The direction of each microplane is defined to be normal to the surface of a sphere centered at the material point (Figure 3). After imposing such constraints, a local constitutive behavior is assumed in order to evaluate the local stresses as well as a microplane measure of the material degradation. In the final stage, macroscopic stresses as well as the global constitutive tensor are evaluated after using an energy principle.

Figure 1 – Discontinuity plans inside concrete microstructure

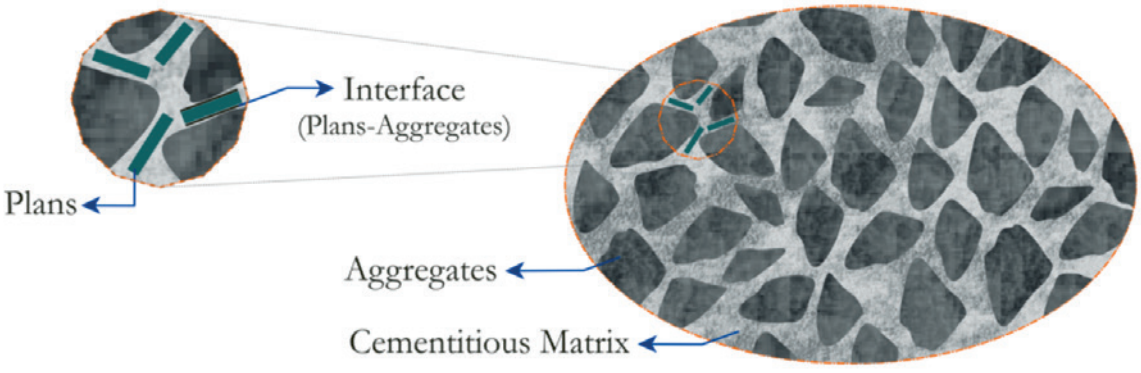

Figure 2 – Synthesis of the Microplane Models formulation

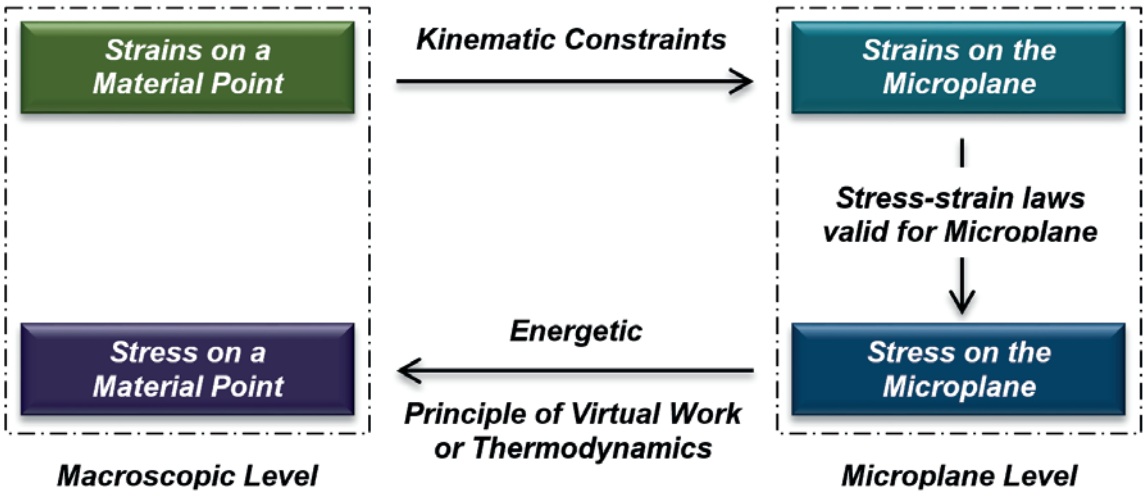

The model proposed by Leukart and Ramm [8] adopts (step 1) a decomposition of the macroscopic strain tensor into its volumetric and deviatoric components (V-D split); (step 2) that the damage process is the main dissipation mechanism which describes the degradation on the material and that degradation is evaluated through a single equivalent strain combined with a single damage law; (step 3) that the free energy on the microplanes exists and its integral over all microplanes is equal to the macroscopic free energy of *Helmholtz*.

Wolenski [9] generalizes the computational implementation of Leukart and Ramm [8] proposition, in order to allow any microplane equivalent strain measure and any damage law. Such an improvement has been implemented in the context of the Unified Computational Environment, proposed by PENNA [11], on the *INSANE* system.

The numerical simulations presented in this paper use one of the options of the unified environment for microplane models of the *INSANE* system. Specifically, the simulations uses volumetric-deviatoric strain split proposed by Leukart and Ramm [8] and the equivalent strain defined by de Vree [12], according to:

$$\eta_{Vree} = 3k_1\varepsilon^V + \sqrt{\left(3k_1\varepsilon^V\right)^2 + \frac{3}{2}k_2\varepsilon_p^D\varepsilon_p^D} \quad (1)$$

where η_{Vree} is equivalent strain measure, ε^V is volumetric part of the strain tensor, ε_p is the *p* component of the deviatoric strain tensor and k_1 and k_2 are material parameters that relate to

Figure 3 – Microplane positions and kinematic constraints

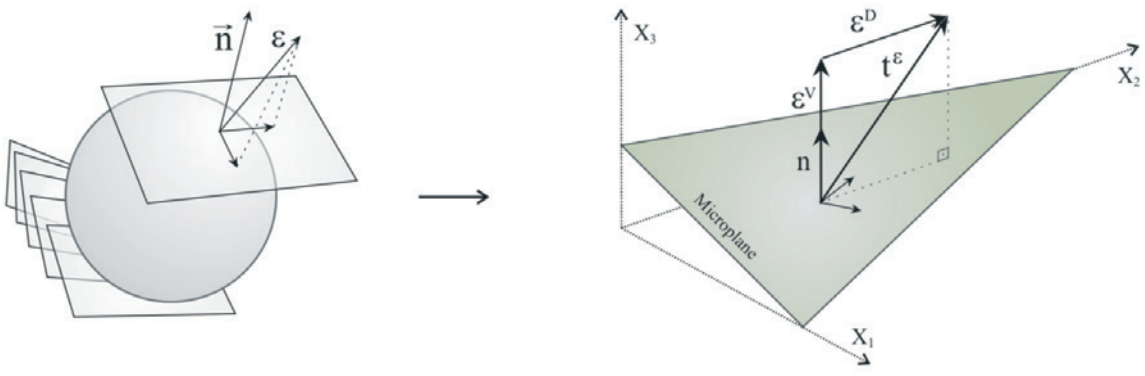

tensile and compression of concrete, and an exponential damage law, given by:

$$d^{mic} = 1 - \frac{\kappa_0}{\kappa}\left\{1 - \alpha + \alpha e^{\left[\beta(\kappa_0 - \kappa)\right]}\right\} \quad (2)$$

where d^{mic} is the damage measure, κ is the current equivalent strain, κ_0 is a material parameter that specifies a limit for κ referring to the beginning of the damage process, and α and β are others material parameters.

3. Reinforcement and bond-slip model

Reinforcement and bond-slip can be represented into reinforced concrete FEM models according to three different approaches: Smeared Reinforcement Models, Discrete Reinforcement Models (Ngo and Scordelis [13]) and Embedded Reinforcement Models (Balakrishna and Murray [14], Allwood and Bajarwan [15] and Elwi and Hrudey [16]).

As can be seen in de Castro [17], the two last approaches were implemented into the *INSANE* system resulting in a powerful tool for the analysis of reinforced concrete structural elements that allows the combination of any constitutive models for concrete and steel, as well as any bond stress-slip law.

The numerical simulations presented in this paper adopt the embedded reinforcement model proposed by Elwi and Hrudey [16], combining with the bond stress-slip laws proposed by Eligehausen [18] and Hawkins [19].

3.1 The finite element with embedded reinforcement

The element proposed by Elwi and Hrudey [16] is composed of an arbitrary element with an embedded reinforcement segment, according to Figure 4 to the bidimensional case.

In this model, the normal strain in the tangent direction to the reinforcement segment is provided by the sum of two components. The first one comes from the deformation of the concrete in the tangent direction to the reinforcement segment and the second one comes from the slip of the reinforcement. The concrete strains are directly obtained from the displacement field of the plane finite element (the parent element) and the reinforcement slip is obtained by interpolating its values at the nodes of the steel segment. The stiffness matrix of the composed element is given by:

$$\begin{bmatrix} [k_{bb}] & [k_{bs}] \\ [k_{sb}] & [k_{ss}] + [k_{cc}] \end{bmatrix} \quad (3)$$

The sub matrix $[k_{cc}]$ is due the constitutive model chosen for representing concrete and the matrices $[k_{ss}]$, $[k_{bb}]$ and $[k_{bs}]$ represent the contributions of steel and bond on the stiffness of the composite element, where:

$$[k_{bb}] = \int_s \left(\{\psi\} E_b \psi O_s + \{B_b\} E_s B_b A_s\right) \cdot t \cdot ds \quad (4)$$

$$[k_{bs}] = [k_{sb}]^T = \int_s \{B_b\} E_s B_s A_s \cdot t \cdot ds \quad (5)$$

$$[k_{ss}] = \int_s \{B_s\} E_s B_s A_s \cdot t \cdot ds \quad (6)$$

In the equations above, the integrals are performed over the line representing the reinforcement layer, and ψ contains the bond slip interpolation functions; E_b is the tangent module of the bond stress-slip law; O_s is the reinforcement perimeter per unit of thick-

Figure 4 – Bidimensional finite element with embedded reinforcement

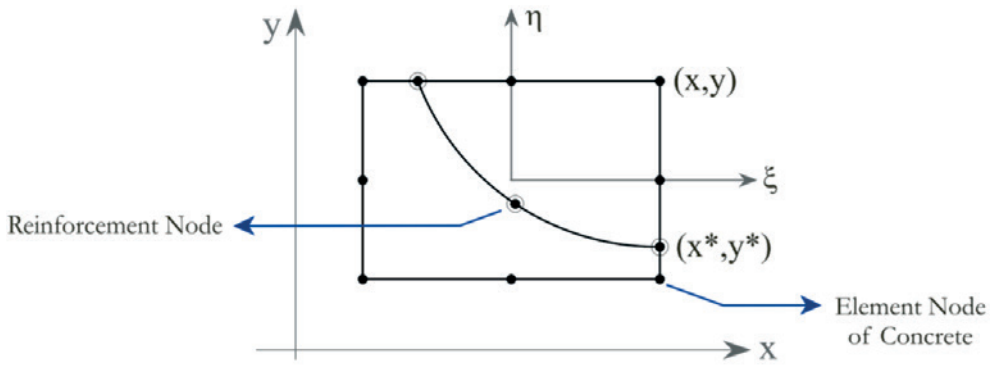

Figure 5 – Bond Stress-Slip law proposed by Eligehausen (18)

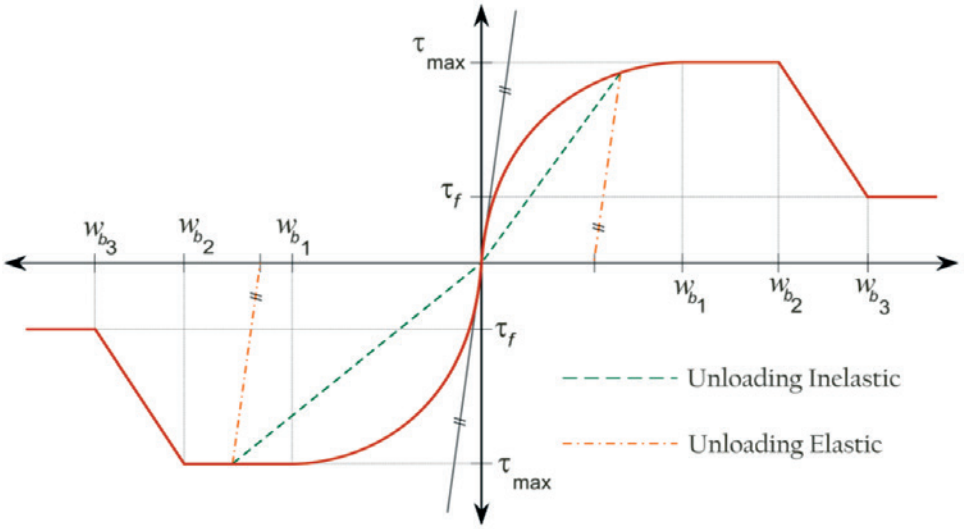

ness; B_b contains the derivatives of the bond slip interpolation functions relative to the tangent direction of the reinforcement layer; E_s is the tangent module of the stress-strain relation for the steel; A_s is the reinforcement area per unit of thickness; t is the element thickness; B_s contains the derivatives of the interpolation functions of the parent element relative to the tangent direction of the reinforcement layer.

3.2 Bond stress-slip laws

As said before, the laws proposed by Eligehausen [18] and Hawkins [19] where used in the numerical simulations presented in this paper. The law proposed by Eligehausen [18] is given by the equations (7) and is illustrated in Figure 5. Hawkins [19] proposed the trilinear law showed in Figure 6.

$$\tau = \tau_{max}\left(\frac{w_b}{w_{b1}}\right)^a \text{ for } 0 \le w_b \ge w_{bmax},$$

$$\tau = \tau_{max} \text{ for } w_{b1} \le w_b \ge w_{b2},$$

$$\tau = \tau_{max} - \left(\tau_{max} - \tau_f\right)\left(\frac{w_b - w_{b2}}{w_{b3} - w_{b1}}\right) \text{ for } w_{b2} \le w_b \ge w_{b3},$$

$$\tau = \tau_f \text{ for } w_b \ge w_{b3} \qquad (7)$$

where τ is the bond stress to a given slip w_b; τ_{max} is the maximum bond stress; τ_f is the final bond stress; w_{b1} is the slip related to the maximum bond stress; w_{b3} is the slip at the moment when the bond stress reaches its end point.

4. Experimental program

The experimental program, presented here, has been performed by Silva [1] and is also described in Silva [20]. The steel-concrete bond was evaluated on two concrete mixtures corresponding to strength classes $25\,MPa$ and $45\,MPa$ (C25 and C45) and three diameters of the steel bars ($8mm$, $10mm$ and $12.5mm$) (reinforced bars type CA-50, ABNT NBR 7480 [21]). For each combination described, six specimens were tested, totaling 108 pull-out tests.

4.1 Materials

For the manufacture of concrete was used cement type CPV-ARI (high early strength Portland cement - ABNT NBR 5733 [22]) with specific mass of $3.05g/cm^3$, specific apparent mass of $0.90g/cm^3$ and specific surface area (Blaine) of $4768cm^2/g$. The fine aggregate was medium sand with fineness modulus of 2.15, specific mass of $2.61g/cm^3$, and maximum nominal size of $4.75mm$. The coarse aggregate was crushed basaltic, with fineness modulus equal to 6.48, specific mass of $2.90g/cm^3$ and a maximum nominal size of $19.0mm$. The additive used was a polycarboxylate-based third-generation superplasticizer, which according to the manufacturer has a density of $1.08g/cm^3$, solid content of 30 and a pH of 4.42.

The slump was fixed at $10 \pm 2cm$. In order to limit the w/c ratio it accepted superplasticizer additive content of 0.26 in relation to the cement mass, for both concrete mixtures. Table 1 shows the mixture proportions of concrete C25 and C45.

To analyze the mechanical properties of concrete were made cylindrical specimens with $10cm$ diameter and $20cm$ high. For each rupture age three specimens were molded, according to ABNT NBR 5738 [23]. They were compacted using a vibrating table completed in two concrete layers of 10s duration per layer. The cure

Figure 6 – Bond Stress–Slip law proposed by Hawkins (19)

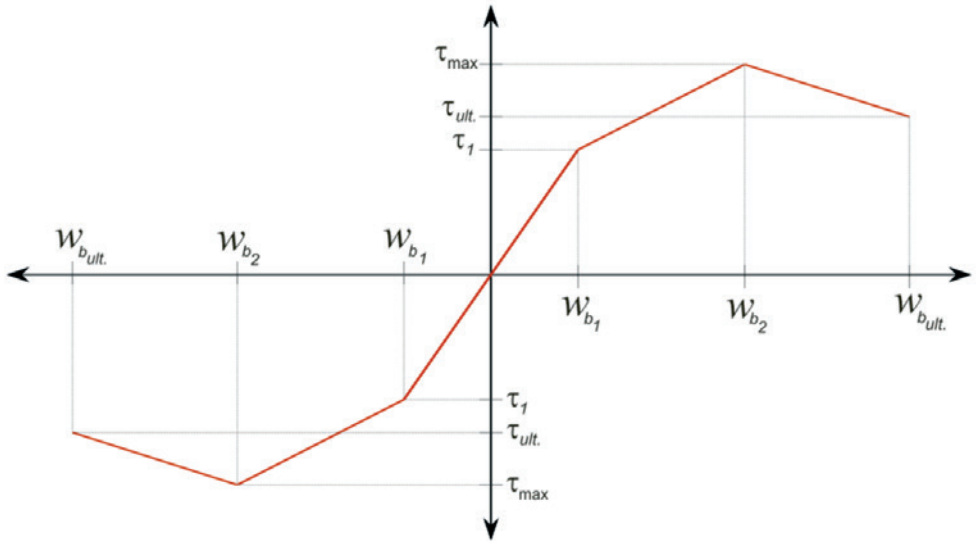

was performed in a humid chamber at relative humidity above 95 and temperature of $23 \pm 2^{o} C$.

To characterize the concrete produced, compressive strength tests were performed according to ABNT NBR 5739 [24]; tensile strength of concrete by diametral compression according to ABNT NBR 7222 [25], and elastic modulus of elasticity of concrete, according to ABNT NBR 8522 [26]. Table 2 shows the results, indicating the average and the standard deviation of the sample consisting of three specimens for each age and type of test.

The ribbed steel bars (type CA-50), used to generate the specimens for the bond tests, were characterized according to ABNT NBR 7480 [21]. This standard specifies that the yield stress of the steel bars is at least $500\,MPa$ and tensile strength is 10% greater than this value. For each diameter ($8mm$, $10mm$ and $12.5mm$), three $60cm$ long specimens were tested. The results are shown in Table 3.

Table 1 – Mixture proportions of concrete (kg / m³)

Material	C25	C45
Cement Portland	318.33	502.99
Fine aggregate	933.65	777.76
Coarse aggregate	958.09	977.01
Water	200.64	192.38
Superplasticizer	0.83	1.31
Water/Cement	0.61	0.37

4.2 *Experimental pull-out test*

The Pull-Out Test (POT) is standardized by RILEM/CEB/FIB [27] and consists of plucking a steel bar integrated into a concrete

Table 2 – Mechanical properties of concrete

Mechanical properties - concrete (28 days)	C25	C45
Compressive strength - f_{cm} (MPa) (Std. dev.)	27.8 (1.6)	49.3 (1.6)
Tensile strength by diametral compression - f_{cfm} (MPa) (Std. dev.)	3.28 (0.23)	4.60 (0.22)
Elastic modulus - E_c (GPa) (Std. dev.)	36.10 (2.82)	46.85 (0.28)

Table 3 – Characterization of the reinforced bars with nominal diameter Ø (mm)

Properties	8.0	10.0	12.5
Yield stress f_y (MPa) (Std. dev.)	625.0 (0.7)	620.0 (2.1)	580.0 (3.1)
Tensile strength f_{st} (MPa)	777.0 (3.5)	782.0 (1.4)	743.0 (2.6)
Linear mass (kg/m)	0.398 (0.004)	0.610 (0.005)	0.956 (0.005)

Figure 7 – Characterization of the pull-out test

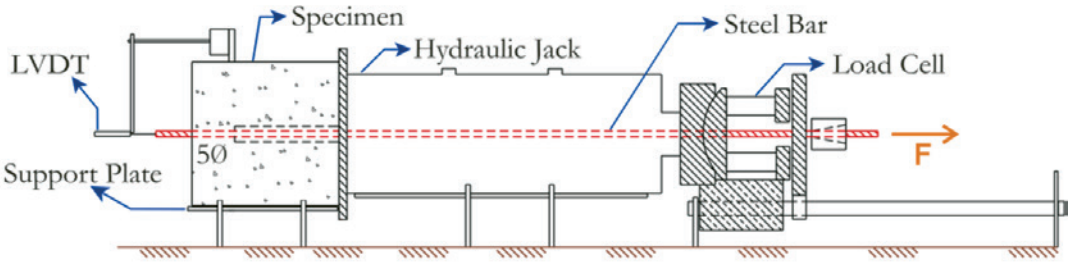

specimen. This test has aimed to study the relationship between bond stress and bond loss of the steel bar. Both ends of the bar are designed for out of the specimen, so that, the pull-out force is applied at one end while the bond loss is measured at the opposite end (Figure 7).

The specimen is cubic with dimension ten times the diameter of the bar ($10Ø$), the minimum size is $20cm$ and the bond length is fixed at five times the diameter of the bar ($5Ø$). Figure 8 shows concreting in the metal mold on a vibrating table and the pull-out specimens.

The system pull-out to method POT was mounted on a movable support properly leveled. For application of force was used a hydraulic jack with a capacity of $600kN$, connected to a manual pump pressure which was applied pulling force at one end of the bar, who reacted against the specimen. Figure 7 illustrates a schematic with the method POT. The pullout force was measured by the load cell and the linear displacement by LVDT.

These data were collected through the data acquisition system (QuantumX) and visualized through the computer program (CatmanEasy), both from HBM. With this system it was possible to obtain the force versus displacement curves.

The bond strength (τ) is calculated according to Equation (8), where F is the pullout force and $\varnothing$ is the diameter of the steel bar.

$$\tau = \frac{F}{5\pi\,\varnothing^2} \qquad (8)$$

Figure 8 – Concreting in metallic mold on a vibrating table (a); specimens POT concreted (b)

Figure 9 – Finite element mesh for the pull-out test

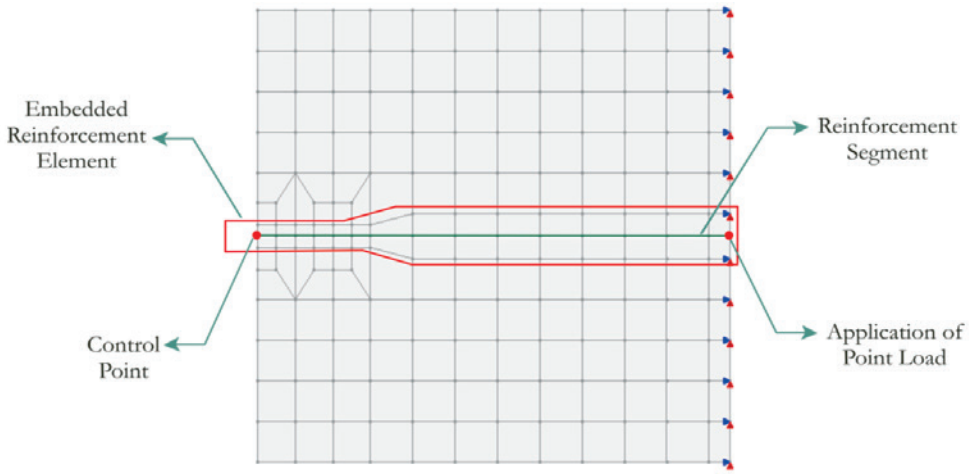

5. Numerical simulations of pull-out test

The pull-out tests above described were simulated using the *INSANE* tools for the analysis of reinforced concrete. The microplane model proposed by Leukart and Ramm [8] combined with the equivalent strain defined by de Vree [12] was used for representing the concrete. The steel was represented by an elastoplastic stress-strain law inside the embedded reinforcement model proposed by Elwi and Hrudey [16], combined with the bond stress-slip laws proposed by Eligehausen [18] and Hawkins [19].

Figure 9 illustrates the finite element mesh adopted: 132 four-node quadrilateral finite elements (with 2 x 2 integration points) to represent the concrete and 15 embedded reinforcement elements (with 2 integration points) to characterize the steel.

According the experimental data, the following material parameters have been adopted: Young's Modulus $E_c = 36100\,MPa$ and Poisson ratio $\nu_c = 0.15$, for concrete **C25**; Young's Modulus $E_c = 46850\,MPa$ and Poisson ratio $\nu_c = 0.20$, for concrete **C45**; Young's Modulus $E_s = 210000\,MPa$ and Yielding Stress $f_y = 625\,MPa$ (8mm), $f_y = 620MPa$ (10mm), $f_y = 580\,MPa$ (12.5mm), for steel.

By fitting the unidimensional behavior observed from the experimental data, it was possible to obtain the numerical parameters to the exponential damage law based on the equivalent strain defined by de Vree [12]. The following values were found (see equation 1 and 2): $\alpha = 0.950$, $\beta = 2200$, for concrete **C25** and **C45**; $\kappa_0 = 0.000103$, $k_1 = 0.630$ and $k_2 = 0.2675$ for **C25**; $\kappa_0 = 0.000103$, $k_1 = 0.7556$ and $k_2 = 0.1943$ for **C45**.

For consideration of bond loss, according to laws proposed by Eligehausen [18] and Hawkins [19], the parameters presented in Tables 4, 5, 6 and 7 were used (Figures 5 and 6).

Table 4 – Parameters for the Eligehausen bond law for concrete C25

Bar of 8.0 mm		
w_{b1} = 0.75 mm	w_{b2} = 1.25 mm	w_{b3} = 5.00 mm
α = 0.40 mm	τ_{max} = 16.50 Mpa	τ_f = 6.00 Mpa
Bar of 10.0 mm		
w_{b1} = 0.45 mm	w_{b2} = 1.00 mm	w_{b3} = 5.00 mm
α = 0.40 mm	τ_{max} = 20.00 Mpa	τ_f = 7.00 Mpa
Bar of 12.5 mm		
w_{b1} = 0.30 mm	w_{b2} = 0.90 mm	w_{b3} = 5.00 mm
α = 0.40 mm	τ_{max} = 22.50 Mpa	τ_f = 9.00 Mpa

Table 5 – Parameters for the Eligehausen bond law for concrete C45

Bar of 8.0 mm		
w_{b1} = 0.30 mm	w_{b2} = 1.00 mm	w_{b3} = 5.00 mm
α = 0.40 mm	τ_{max} = 23.50 Mpa	τ_f = 9.00 Mpa
Bar of 10.0 mm		
w_{b1} = 0.30 mm	w_{b2} = 1.00 mm	w_{b3} = 5.50 mm
α = 0.40 mm	τ_{max} = 26.00 Mpa	τ_f = 12.50 Mpa
Bar of 12.5 mm		
w_{b1} = 0.30 mm	w_{b2} = 1.00 mm	w_{b3} = 6.00 mm
α = 0.40 mm	τ_{max} = 29.00 Mpa	τ_f = 15.50 Mpa

Table 6 – Parameters for the Hawkins bond law for concrete C25

Bar of 8.0 mm		
w_{b1} = 0.25 mm	W_{b2} = 1.15 mm	w_{bult} = 4.85 mm
τ_1 = 11.50 mm	τ_{max} = 16.50 Mpa	τ_{ult} = 6.00 Mpa
Bar of 10.0 mm		
w_{b1} = 0.10 mm	w_{b2} = 0.75 mm	w_{bult} = 5.10 mm
τ_1 = 13.00 mm	τ_{max} = 20.00 Mpa	τ_{ult} = 7.00 Mpa
Bar of 12.5 mm		
w_{b1} = 0.10 mm	w_{b2} = 0.60 mm	w_{bult} = 5.30 mm
τ_1 = 16.50 mm	τ_{max} = 22.50 Mpa	τ_{ult} = 9.00 Mpa

Table 7 – Parameters for the Hawkins bond law for concrete C45

Bar of 8.0 mm		
w_{b1} = 0.10 mm	w_{b2} = 0.75 mm	w_{bult} = 4.85 mm
τ_1 = 17.00 mm	τ_{max} = 23.50 Mpa	τ_{ult} = 9.00 Mpa
Bar of 10.0 mm		
w_{b1} = 0.10 mm	w_{b2} = 1.10 mm	w_{bult} = 5.20 mm
τ_1 = 23.50 mm	τ_{max} = 27.00 Mpa	τ_{ult} = 12.50 Mpa
Bar of 12.5 mm		
w_{b1} = 0.10 mm	w_{b2} = 0.90 mm	w_{bult} = 6.10 mm
τ_1 = 27.50 mm	τ_{max} = 29.00 Mpa	τ_{ult} = 15.50 Mpa

Figure 10 – Experimental and FEM results for concretes C25 and C45 and reinforcing bars of 8mm, 10mm and 12.5mm

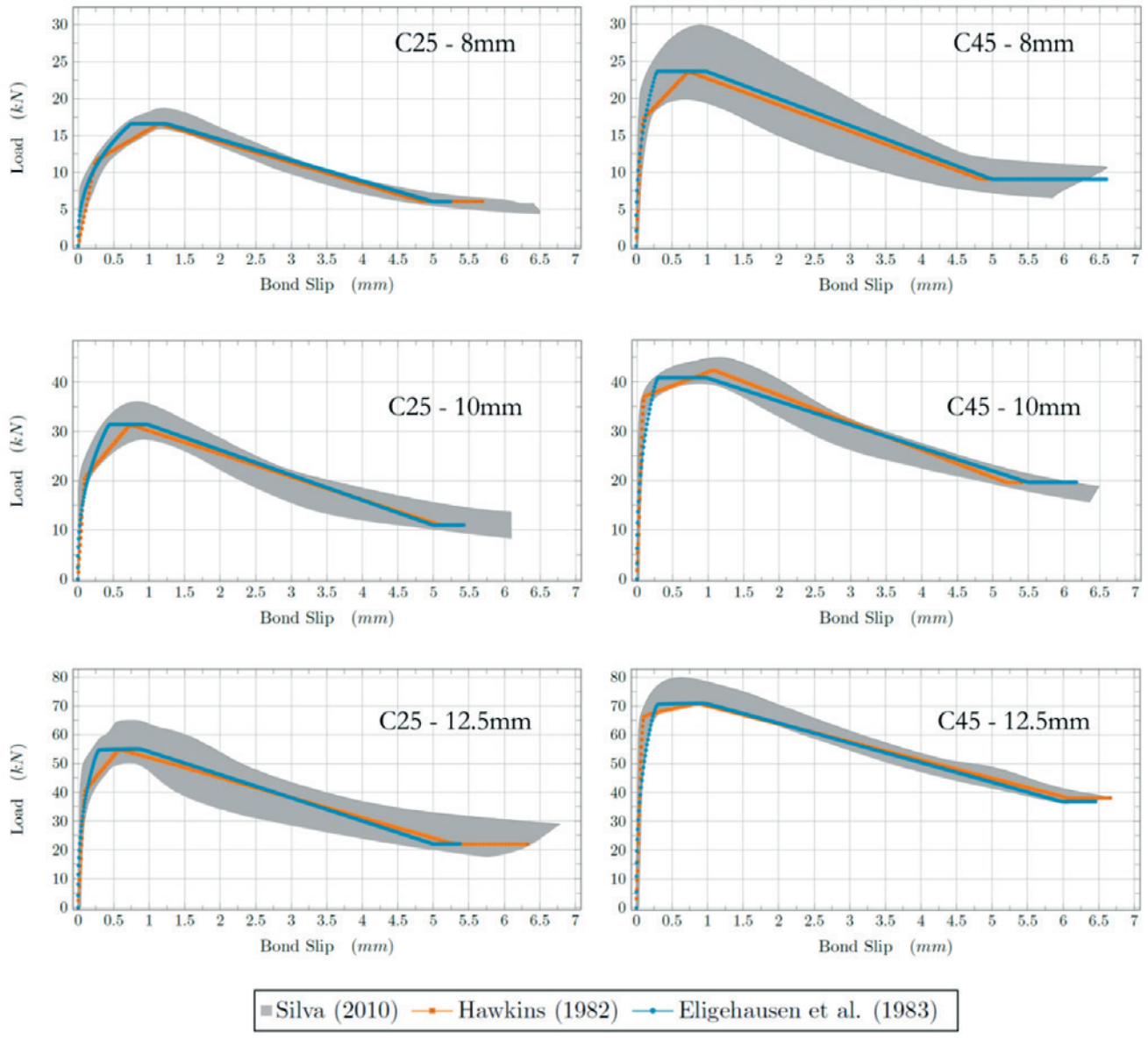

Figure 11 – FEM results for bond stress×slip curves for Eligehausen (E) and Hawkins (H) bond laws

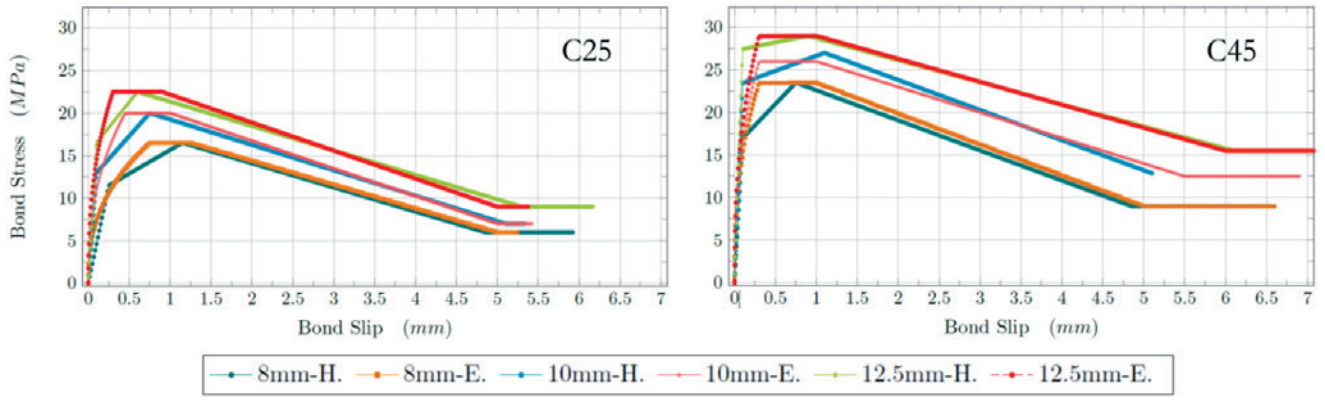

Nonlinear simulations have been performed under the assumption of plane stress conditions and using generalized displacement control method (Yang and Shieh [28]), initial load factor equal to 0.080 and 0.040 for Eligehausen [18] and Hawkins [19] bond laws, respectively, and tolerance of 1×10^{-4}.

The results of the numerical simulations, together the range of experimental data, can be seen in Figure 10, referring to concrete **C25** and **C45**, and to bar diameters of $8mm$, $10mm$ and $12.5mm$. Figure 10 shows good agreement between the experimental and numerical results for the six combinations of two concretes and three reinforcing bars. Both, the Eligehausen and Hawkins laws represented well the experimental range. Clearly, the Eligehausen law has represented better because of its nonlinear nature. This feature was very important, mainly for load levels near of the load limits, when the behavior is strongly nonlinear.

The curves bond stress × slip for all simulations can be seen in Figure 11. By comparing Figures 11 and 10, it can be observed that the curves load × slip (Fig. 10) and bond stress × slip (Fig. 11) have the same shapes. It is also observed that the bond stress and slip limits of the Figure 11 are almost equals to the ones used as input values (Tables 4, 5, 6 and 7). These observations allows to conclude that structural behavior of the test and the local behavior of the concrete-steel interface are almost the same, highlighting the pertinence of the RILEM's test to study local interactions between the two materials. The observations also allow concluding that, despite the sophistication of the constitutive model used for concrete, it was not so important for this FEM analysis.

In spite of good agreement between experimental and FEM analysis, as showed in Figure 10, the FEM results for C45-12.5mm were obtained using a lower limit of bond stress ($29\,MPa$). For all analysis performed with bond stress limit larger than $29\,MPa$ the incremental-iterative process stops at the same load level ($71.176\,kN$), as illustrated in Figure 12 (points A and B).

Figure 12 – Experimental and FEM results for concrete C45 and reinforcing bars of 12.5mm

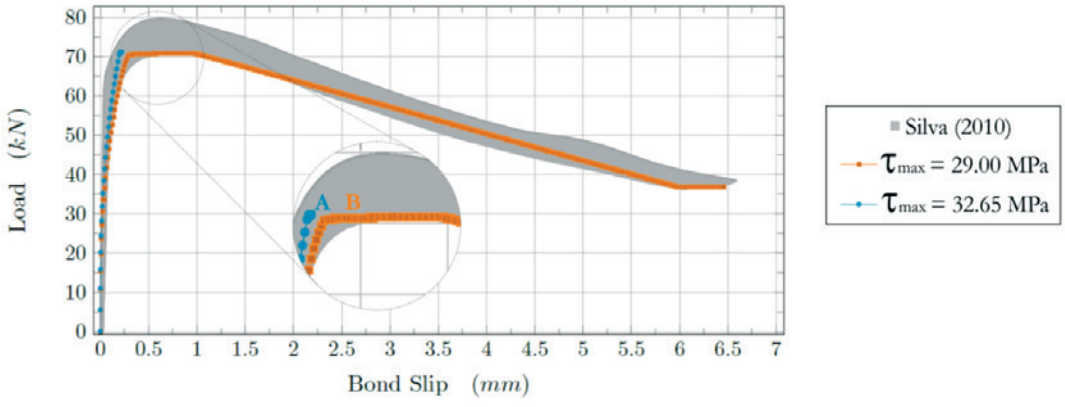

Figure 13 – Mesh's deformed shape and variation of the reinforcement force, bond stress and reinforcement slip, corresponding to the points A and B of the Figure 12

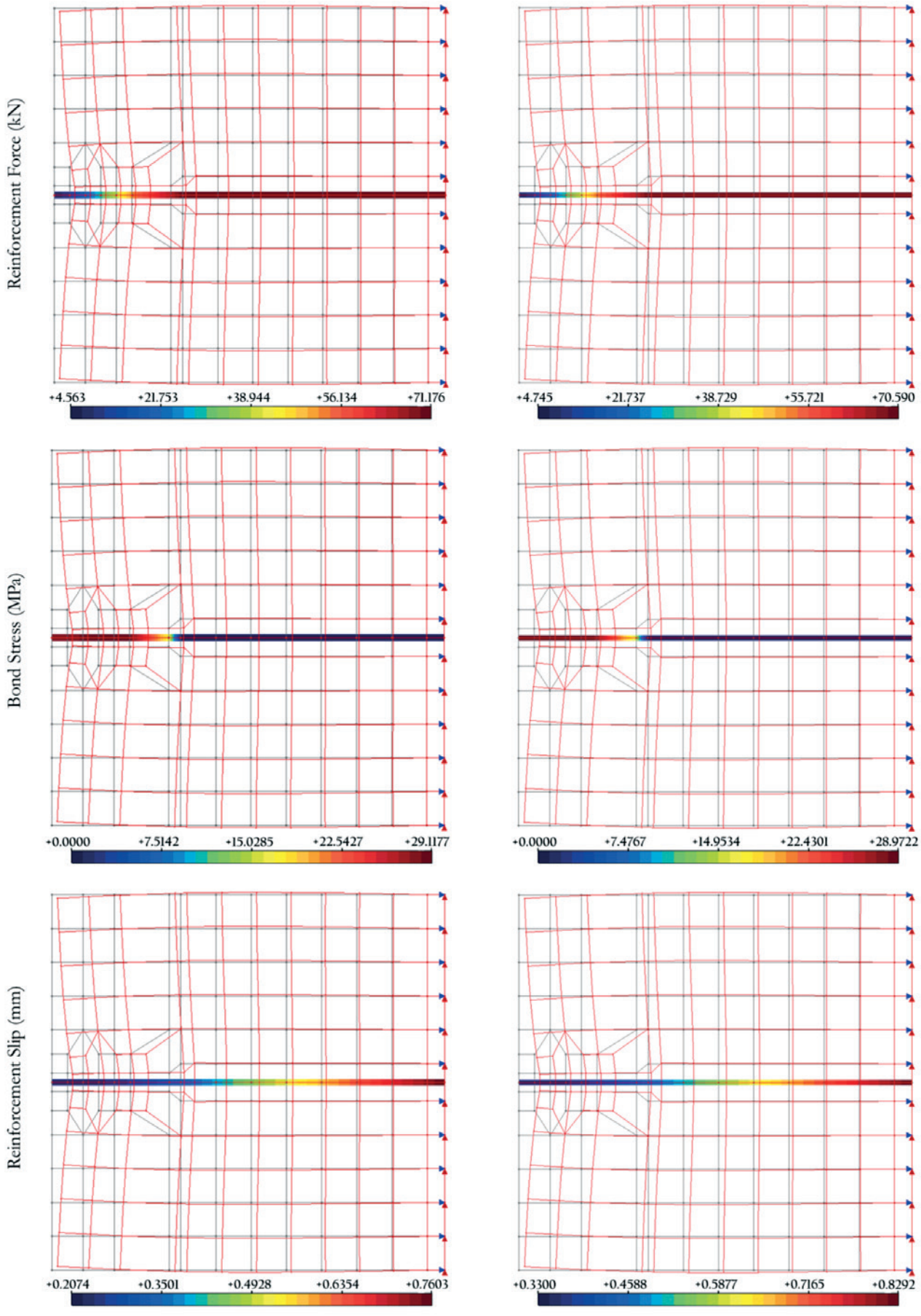

In order to explain this occurrence, Figure 13 shows the variation of the reinforcement force, bond stress and reinforcement slip, as well as the mesh's deformed shape, corresponding to the points A (right images) and B (left images) of the Figure 12.

As can be seen in Figure 13, the maximum values for reinforcement force, bond stress and reinforcement slip are: $71.176\,kN$, $29.1177\,MPa$ and $0.7603\,mm$ for point A (see Fig. 12), and $70.590\,kN$, $28.9722\,MPa$ and $0.8292\,mm$ for point B (see Fig. 12). These values, as well as the general behavior illustrated in Figure 13, are very close to the input data of Table 7, highlighting again the local nature of the phenomenon. Also, it is observed that the reinforcement force for point A ($71.176\,kN$) corresponds to the steel yield stress, according with experimental values (Table 3), and this is the reason because the incremental-iterative process stops. So, this analysis allows concluding that, for this case (C45-$12.5\,mm$), the reinforcement yielding limits the development of transfer mechanisms at the interface steel-concrete.

Although, it was noted the occurrence, for all experimental tests for this case (C45-$12.5mm$), of the failure by pullout, the experimental values in Table 3, shows that this failure was on the threshold of the steel yield strength, contributing to the statement obtained from the numerical simulations presented.

6. Final remarks

The numerical results obtained from the use of Microplane Constitutive Model combined with an Embedded Reinforcement Model and two bond stress-slip laws were compared with the experimental results and a good agreement was observed.

Also was observed a good representation of the actual behavior of the RILEM/CEB/FIB [27] Pull-Out test, using the proposed combination, highlighting the pertinence of the RILEM proposal to study the local behavior of the concrete-steel interface.

A correlation between numerical and experimental results and some parameters validates the proposed combination and identifies the significance of such parameters on response.

So, it can conclude that such combination enables a realistic representation of the behavior of the bond loss between the reinforcement and concrete.

In the simulations of the RILEM's tests presented in this paper, the concrete constitutive model was not so important due the local nature of such tests. However, the combined effects of concrete nonlinearity and bond-slip are very important and should always be included in general finite element models because, in damaged regions, there are peaks of bond stress due to the intensification of transfer effort at the interface between cracked areas and intact ones.

Aiming to expand the knowledge about this theme, new simulations must be performed using the *INSANE* tools for reinforced concrete structures, such as: the extensive library of constitutive models for concrete, the discrete approach models for reinforcement including interface finite elements for bond slip consideration.

7. Acknowledgements

The authors gratefully acknowledge the important support of FAPEMIG (in Portuguese "Fundação de Amparo à Pesquisa de Minas Gerais" - Grant PPM-00310-13), FAPESP (in Portuguese "Fundação de Amparo à Pesquisa do Estado de São Paulo" - Processo 08/57743-7) and of CNPq (in Portuguese "Conselho Nacional de Desenvolvimento Científico e Tecnológico" – Grant 308785/2014-2).

8. Nomenclature

F - Pullout force (kN);
Ø - Diameter of steel bar (mm);
E_c - Elastic modulus of elasticity of concrete (GPa);
POT - **P**ull-**O**ut **T**est (RILEM/CEB/FIP RC6: 1983);
f_{cm} - Compressive strength of concrete average (MPa);
f_{ctm} - Tensile strength of concrete by diametral compression average (MPa);
f_y - Yield stress of steel (MPa);
f_{st} - Tensile strength of steel (MPa);
τ - Steel-Concrete Bond strength (MPa);
$\tau_{máx}$ - Steel-Concrete Maximum bond strength (MPa);
τ_1 - Steel-Concrete initial bond strength (MPa);
$\tau_{ult.}$ - Steel-Concrete ultimate bond strength (MPa).

9. References

[1] SILVA, B. V. Investigação do Potencial dos Ensaios Apulot e Pull-Out para Estimativa da Resistência a Compressão do Concreto. Master's Thesis. Universidade Estadual Paulista (UNESP), Ilha Solteira, SP, Brazil, 2010.

[2] MOHR, O. Welche Umstände Bedingen die Elastizitätsgrenze und den Bruch Eines Materiales? 1900. Cited in Leukart [7].

[3] TAYLOR, G. I. Plastic Strains in Metals. Journal of the Institute of Metals, v. 62, p. 307-324, 1938. Cited in Leukart [7].

[4] BAŽANT, Z. P.; GAMBAROVA, P. G. Crack Shear in Concrete: Crack Band Microplane Model. Journal of Structural Engineering, v. 110, p. 2015-2035, 1984.

[5] CAROL I.; JIRÁSEK M.; BAŽANT Z. P. A thermodynamically consistent approach to microplane theory. I. Free energy and consistent Microplane stresses. International Journal of Solids Structures, v. 38, p. 2921-2931, 2001.

[6] OŽBOLT J.; LI Y.; I. KOŽAR. Microplane model for concrete with relaxed kinematic constraint. International Journal of Solids Structures, v. 38, p. 2683-2711. 2001.

[7] C AROL I.; JIRÁSEK M.; BAŽANT Z. P. A framework for microplane models at large strain, with application to hyper elasticity. International Journal of Solids Structures, v. 41, p. 511-557, 2004.

[7] LEUKART, M. Kombinierte Anisotrope Schädigung und Plastizität bei Kohäsiven Reibungsmaterialien. Ph.D. Thesis, Universität Stuttgart, German, 2005.

[8] LEUKART, M.; RAMM, E. Identification and Interpretation of Microplane Material Laws. Journal of Engineering Mechanics, v. 132, p. 295-305, 2006.

[9] WOLENSKI, A. R. V. Ambiente Teórico-Computacional Unificado para Modelos Constitutivos: Inclusão de Modelo de Microplanos. Master's Thesis. Universidade Federal de Minas Gerais (UFMG), Brazil, 2013.

[10] WOLENSKI, A. R. V.; MONTEIRO, A. B.; PENNA, S. S.; PITANGUEIRA, R. L. S. Simulações Numéricas de Estruturas de Concreto Usando um Modelo de Microplanos. In.: 55º Congresso Brasileiro do Concreto. Gramado, RS, Brazil, 2013.

[11] PENNA, S. S. Formulação Multipotencial para Modelos de Degradação Elástica: Unificação Teórica, Proposta de Novo Modelo, Implementação Computacional e Modelagem de Estruturas de Concreto. Ph.D. Thesis. Universidade Federal de Minas Gerais (UFMG), Brazil, 2011.

[12] de VREE, J. H. P.; BREKELMANS, W. A. M.; van GILS, M. A. J. Comparison of nonlocal approaches in continuum damage mechanics. Computer and Structures, v. 55, p. 581-588, 1995.

[13] NGO, D.; SCORDELIS, A. C. Finite element analysis of reinforced concrete beams. Journal of ACI, v. 64, p. 152-163, 1967.

[14] S. BALAKRISHNA; D. W. MURRAY. Prediction of response of concrete beam sand panels by nonlinear finite element analysis. IABSE Reports, p. 393-404, 1987.

[15] R. J. ALLWOOD; A. A. BAJARWAN, A new method for modelling reinforcement and bond in finite element analysis of reinforced concrete, International Journal of Numerical Methods in Engineering, v. 26 p. 833-844, 1989.

[16] ELWI, A. E.; HRUDEY, T. M. Finite Element Model for Curved Embedded Reinforcement. Journal of Engineering Mechanics, v. 115, p. 740 754, 1988.

[17] de CASTRO, S. S. Framework Teórico e Computacional para Estruturas de Concreto Armado: Implementação de Modelos de Armadura e Aderência. Master's Thesis. Universidade Federal de Minas Gerais (UFMG), Brazil, 2013.

[18] ELIGEHAUSEN, R., POPOV, E. P., BERTORO, V. V., Local Bond Stress-Slip Relationships of Deformed Bars Under Generalized Excitations. Earthquake Engineering Research Centre, University of California, Berkeley, p. 169, 1983.

[19] HAWKINS, N.; LIN, I. J.; JEANG, F. L. Local Bond Strength of Concrete for Cyclic Reversed Loadings, 1982.

[20] SILVA, B. V.; BARBOSA, M. P.; SILVA FILHO, L. C. P.; LORRAIN, M. S. Experimental investigation on the use of steel-concrete bond tests for estimating axial compressive strength of concrete: part 1. Revista IBRACON de Estruturas e Materiais, v. 6, p. 715-736, 2013.

[21] ASSOCIAÇÃO BRASILEIRA DE NORMAS TÉCNICAS. NBR 7480: Aço destinado a armaduras para estruturas de concreto armado - Especificação. Rio de Janeiro, 2007 [In Portuguese].

[22] ASSOCIAÇÃO BRASILEIRA DE NORMAS TÉCNICAS. NBR 5733: Cimento Portland de alta resistência inicial. Rio de Janeiro, 1991 [In Portuguese].

[23] ASSOCIAÇÃO BRASILEIRA DE NORMAS TÉCNICAS. NBR 5738: Concreto - Procedimento para moldagem e cura de corpos de prova. Rio de Janeiro, 2003 [In Portuguese].

[24] ASSOCIAÇÃO BRASILEIRA DE NORMAS TÉCNICAS. NBR 5739: Concreto - Ensaios de compressão de corpos de prova cilíndricos. Rio de Janeiro, 2007 [In Portuguese].

[25] ASSOCIAÇÃO BRASILEIRA DE NORMAS TÉCNICAS. NBR 7222: Concreto e Argamassa - Determinação da resistência à tração por compressão diametral de corpos de prova cilíndricos. Rio de Janeiro, 2010 [In Portuguese].

[26] ASSOCIAÇÃO BRASILEIRA DE NORMAS TÉCNICAS. NBR 8522: Concreto - Determinação do módulo estático de elasticidade à compressão. Rio de Janeiro, 2008 [In Portuguese].

[27] RILEM/CEB/FIB. Bond Test for Reinforcing Steel: Pull-Out Test - RC 6. Comité Euro-International Du Béton, Paris. 1983.

[28] YANG, Y. B.; SHIEH, M. S. Solution method for nonlinear problems with multiple critical points. AIAA Journal, v. 28, p. 2110-2116. 1990.